The Mechanism of Electron Spin Decoherence in a Partially Deuterated Glassy Matrix

Samuel M. Jahn,[†] Elizabeth R. Canarie,[†] and Stefan Stoll[*]

Department of Chemistry, University of Washington, Seattle, Washington 98195, United States

E-mail: stst@uw.edu

Abstract

Long electron spin coherence lifetimes are essential for applications in quantum information science and electron paramagnetic resonance, for instance for nanoscale distance measurements in biomolecular systems using double electron–electron resonance. We experimentally investigate the decoherence dynamics under the Hahn echo sequence of the organic radical d_{18}-TEMPO in a variably deuterated frozen water:glycerol matrix. The coherence time (phase memory time) T_M scales with proton concentration as $[^1H]^{-0.65}$. For selectively deuterated matrices, decoherence is accelerated in the presence of proton clustering, i.e. substantial short-range density in the proton–proton radial distribution functions (< 3 Å). Simulations using molecular dynamics and many-body spin quantum dynamics show excellent agreement with experiment and show that geminal proton pairs such as CH_2 and OH_2 groups are major decoherence drivers. This provides a predictive tool for designing molecular systems with long electron spin coherence times.

TOC Graphic

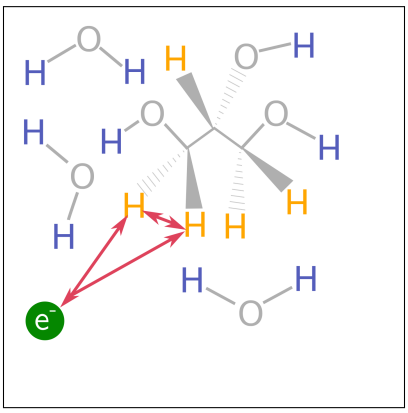

In pulse EPR (Electron Paramagnetic Resonance) spectroscopy and in some quantum sensing applications, coherent pulse excitation schemes of electron spins are used to obtain information about the local environment of unpaired electrons. In these schemes, electron spin coherence is generated at the beginning of the pulse sequence, and it is refocused and detected at the end in the form of a spin echo. An essential requirement is an electron spin coherence time long enough that the generated coherence survives until detection. The presence of nearby magnets (other electrons and magnetic nuclei) modulates the echo amplitude, and if these modulations are resolved, they provide valuable structural insight.[1–3] However, many unresolved modulations lead to irreversible decoherence and loss of echo amplitude.[4,5] Similar balancing problems also occur when using electron spins as qubits; complex calculations require coupling multiple qubits together, but other undesired couplings cause decoherence, limiting the time available for computations.[6]

At temperatures low enough for most motional degrees of freedom to have frozen out, and at sufficiently low electron spin concentrations, the primary decoherence pathway for electron spins in non-T_1-limited systems is via the surrounding bath of coupled nuclear spins, communicated to the electron by hyperfine couplings.[5,7–9] The decoherence timescale depends on the system and the pulse sequence.[5,10,11] For dilute nitroxides in a water:glycerol matrix at 20 K under a Hahn echo sequence, the coherence time (phase memory time) T_{M} is about 5 µs.

Decoherence from bath spins can be strongly reduced by using approximately spin-free or spin-dilute environments. A prime example are nitrogen–vacancy centers in diamond. The low 1.1 % natural abundance for ^{13}C provides long T_{M}s,[12,13] and reducing the ^{13}C concentration further increases the coherence time.[14] For molecular systems, hydrogen-free molecules in matrices such as CS_2 can be used.[15] Another approach is the use of deuterated molecules and solvents.[16,17] This replaces the large magnetic moments of the protons for the smaller magnetic moments of deuterons. The smaller hyperfine couplings, combined with the detuning effect of deuteron electric quadrupole couplings, prolongs the coherence timescale.[18,19]

It is important to understand and be able to predict a priori the decoherence dynamics of electron spins. Such an improved mechanistic understanding is practically relevant, as it provides guidance for avoiding systems with short electron spin coherence times that limit resolution in pulse EPR experiments, sensitivity in quantum sensing, and the number of operations in quantum algorithms.

Here, we investigate the electron spin decoherence in a system where T_{M} is limited by proton spins as a function of proton concentration and distribution, using a frozen dilute solution of the nitroxide radical d_{18}-TEMPO (Figure 1) in 1:1 mass:mass water:glycerol. We measure the electron spin decoherence dynamics under the Hahn echo pulse sequence. We find that the coherence time scales with the proton concentration as $[^1\mathrm{H}]^{-0.65}$, but also depends significantly on the proton–proton radial distribution function.

To rationalize the experimental observations and to develop a predictive model, we employ in silico modeling. There are a number of theoretical methods developed to model nuclear-spin-driven electron spin decoherence, from semi-classical approaches that model the nuclear spin bath as a source of stochastic magnetic noise (requiring the choice of a characteristic timescale)[4,20–23] to many-body quantum dynamics models with the advantage that the timescale emerges from the model.[24–35] Here, we employ the ensemble cluster correlation expansion (CCE) approach[28,29] in combination with molecular dynamics (MD). We have successfully employed this approach on proton-only systems in previous publications.[9,36]

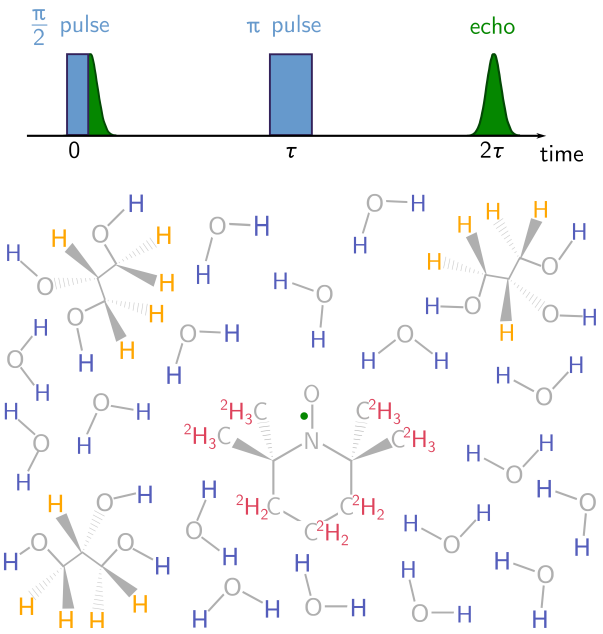

Figure 1: **Top:** Measuring the Hahn echo amplitude as a function of total pulse sequence length, 2τ, provides the simplest way to observe decoherence effects. **Bottom:** The system under study is d_{18}-TEMPO (unpaired electron shown in green) solvated in a frozen 1:1 mass:mass ($\approx$ 5:1 mole:mole) water:glycerol solution, with solvent exchangeable hydrons (blue), solvent non-exchangeable hydrons (yellow) and TEMPO's deuterons (red) contributing to decoherence.

We measured Hahn echo decays as a function of solvent proton concentration, utilizing appropriate mixtures of D_2O:d_8-glycerol and natural-abundance H_2O:h_8-glycerol. To minimize instantaneous diffusion, the d_{18}-TEMPO concentration was kept low at 5 μM. At this concentration, the predicted instantaneous diffusion timescale is $T_{\mathrm{ID}} = 1.6$ ms,[37] much longer than any decoherence time scale observed in this work. To eliminate decoherence contributions from thermal motions and spin–lattice relaxation, echo decays were measured at 20 K. Decoherence contributions from the TEMPO methyl groups are minimal due to methyl perdeuteration.

The experimental Hahn echo decays are shown in Figure 2 (top). The observed decays are of stretched-exponential form. The initial 8 and 16 MHz modulation is independent of solvent proton concentration and is therefore attributed to ESEEM (electron spin echo envelope modulation) from TEMPO deuterons. As deuteration is increased and the proton concentration decreases, the decay timescale increases from about 5 μs at 111.4 M protons (natural abundance) to 70 μs at 1 M protons.

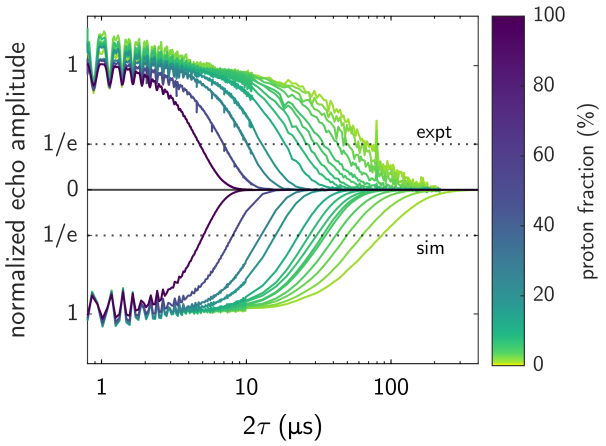

Figure 2: Experimental Hahn echo decays (upper part; 20 K, 1.2 T, 33.8 GHz) and simulated decays (lower part; reflected), are shown as a function of proton fraction (color-coded), for 5 μM d_{18}-TEMPO in a 1:1 water:glycerol matrix where the proton concentration was varied between natural abundance and 1 M via the ratio of H_2O:h_8-glycerol to D_2O:d_8-glycerol.

Figure 2 (bottom) shows explicit quantum spin dynamics simulations based on a structure of the solvated radical obtained by molecular dynamics. The resulting simulated decays are in good agreement with experiment. This is remarkable, since the many-body quantum simulation is exclusively based on the MD structure and does not include any adjustable parameters. The simulations include the electron spin and about 1200 surrounding protons (via periodic boundary conditions; see SI) and use a modified CCE approach. While full CCE converges to the exact result, truncation at a maximum cluster size can give reasonably good approximations. Here, we choose 2-CCE as a compromise between numerical accuracy and computational cost. This leaves some $\mathcal{O}(\tau^3)$ terms unaccounted for.[26,28] The 2-CCE level appears to get within 20% of the correct timescale.

Excluding the ESEEM-affected initial parts, the experimental and simulated decays of Figure 2 are well fit by stretched exponentials of the form

$$V(2\tau) = V_0 \cdot \mathrm{e}^{-(2\tau/T_\mathrm{M})^\xi} \tag{1}$$

with coherence time or phase memory time T_M, initial amplitude V_0, and stretching exponent ξ. Figure 3 plots the fitted T_M and ξ against the proton concentration. (The fits are shown in the SI.) It reveals good agreement between experiment and computational prediction for both T_M and ξ, although the simulations overestimate T_M by about 20 %. To assess the contribution of deuterons to T_M, Figure 3 also compares simulations with and without the deuterons in the system (see SI). The results show that T_M is noticeably affected by deuterons only at $[^1\mathrm{H}] < 3$ M. At higher proton concentrations, the effect of solvent deuterons, or their absence, on decoherence is negligible.

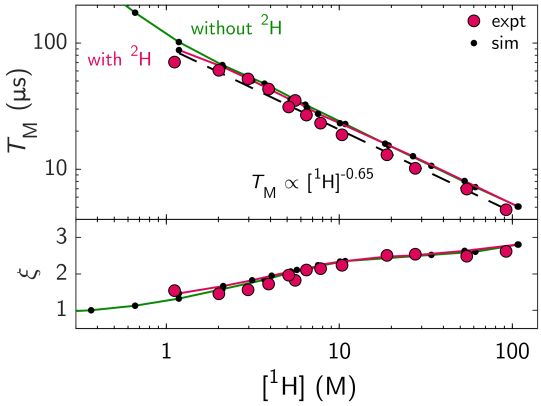

Figure 3: Coherence time (top) and stretching exponent (bottom) are plotted versus proton concentration for the experimental and simulated data from Figure 2. The 95 % confidence intervals are smaller than the circle size. The dashed black line is a fit of Eq. (2) to the experimental data with $T_{\mathrm{M,1M}} = 93 \pm 10\,\mu\mathrm{s}$ and $p = 0.65 \pm 0.05$ ($R^2 = 0.99$). Small black dots indicate fits to the computational predictions, either including deuterons (red line) or excluding them (green line).

Figure 3 shows that ξ is concentration dependent, varying between 1.5 and 2.6. This indicates that it is not strictly possible to infer the decoherence mechanism from the value of ξ, as sometimes done in the literature, where values less than 2 have been associated with methyl rotation or instantaneous diffusion.[18,38] Figure 3 also shows that the experimental T_{M} decreases almost linearly with increasing concentration in this log–log plot, indicating a

$$T_{\mathrm{M}} = T_{\mathrm{M,1M}} \cdot ([^1\mathrm{H}]/\mathrm{M})^{-p} \tag{2}$$

relationship, where $T_{\mathrm{M,1M}}$ is the coherence time at 1 M proton concentration, $[^1\mathrm{H}]/\mathrm{M}$ is the proton concentration divided by a reference 1 molar concentration, and the exponent p is the negative slope in the log–log plot, i.e. $p = -\mathrm{d}\ln T_{\mathrm{M}}/\mathrm{d}\ln([^1\mathrm{H}]/\mathrm{M})$. The fit to the experimental T_{M} data yields $p = 0.65(5)$ ($R^2 = 0.99$), and the simulated data are fit with $p = 0.639(5)$ ($R^2 = 0.999$), again showing that the simulations recover the observations well.

Expectations for p are mixed. On one hand, $p < 1$ is consistent with our earlier work on 3-maleimido-proxyl, where we observed a similarly shallow dependence in the refocused Hahn echo.[36] Experimental T_{M} data on P donors in Si crystals show a $p \approx 0.85$ dependence on the ^{29}Si mole fraction between 4.7 % and 99.2 %.[39] On the other hand, a $[^1\mathrm{H}]^{-1}$ ($p = 1$) fit has previously worked for data where [^{1}H] was varied by solvent type.[18] A $p = 1$ dependence is also expected from analogy with electron spin decoherence driven by electrons (experimentally,[40] and from simulations[41]) or ^{13}C simulations.[42,43]

A simple analytical model for the coherence decay $V(2\tau)$ can be derived under the assumptions that the electron–proton radial distribution function (rdf) $g(R)$ and the proton–proton radial distribution function $g(r)$ are concentration-independent (see SI). By comparison with Eq. (1), the model predicts $p \approx 2/\xi$. Taking the simple model to the low-concentration limit, where both radial distribution functions can be further approximated as scale invariant ($g(R) = g(r) = 1$), the model predicts $p = 1$.

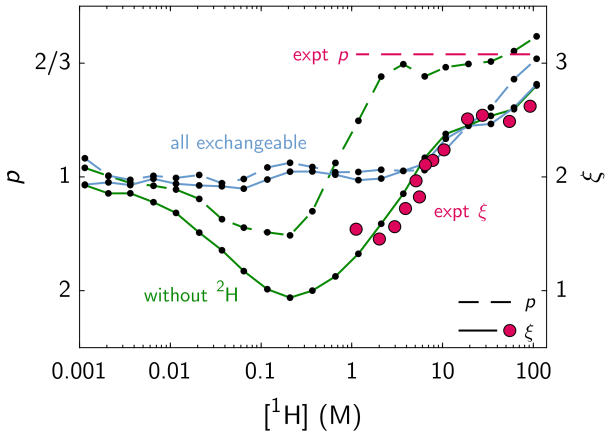

Figure 4: Plot of p (left axis, dashed lines) and ξ (right axis, solid lines) vs. $[^1\mathrm{H}]$ shows three cases, the ξ fitted from experiment (red points) and $p = 0.65$ (red dashed), p and ξ for the simulations series without deuterons (green), and p and ξ of another simulation (again without deuterons), where all hydrons are treated as exchangeable (blue). The simple model prediction $\xi \approx 2/p$ is used to relate the p and the ξ axis. Note that only the fully exchangeable simulations match the simple model's prediction.

Both the $p \approx 2/\xi$ and the $p = 1$ predictions are inconsistent with the observations, as shown in Figure 4. To further explore the connection between our observations and the model predictions, Figure 4 extends the deuteron-free simulations to proton concentrations lower than achievable experimentally. (Even if such low proton concentrations were feasible, the deuterons would dominate the coherence time in this regime.) As the proton concentration decreases, p approaches 1 (dashed lines), as predicted by the simple model. The figure also shows simulations with the assumption that all hydron sites are individually exchangeable. This is helpful for illustrating the importance of glycerol protons exchanging in groups of five. This yields the $p \approx 1$ low-concentration limit over a larger concentration range. Figure 4 also compares the ξ values from fits with Eq. (1) (solid lines), with the model prediction of $2/p$ (dashed lines). There is a clear discrepancy, except for the all-exchangeable series. This indicates that the assumptions underlying the analytical model, i.e. the concentration independence of $g(r)$, are not adequate for these samples.

The above analysis suggests that the ^{1}H–^{1}H rdf $g(r)$ is important in determining the decoherence dynamics. To experimentally investigate the effects of $g(r)$ on T_M, we selectively varied $[^1\mathrm{H}]$ in either the pool of exchangeable hydrons (OH of water and glycerol; using d_5-glycerol/H_2O with d_8-glycerol/D_2O) or the pool of non-exchangeable hydrons (CH_5 in glycerol; using d_3-glycerol/D_2O with d_8-glycerol/D_2O), keeping the other pool maximally (99 %) deuterated. Hydrons disperse evenly across all exchangeable OH sites with a rate constant of 10^9 to 10^{10} $M^{-1}s^{-1}$,[44,45] whereas hydrons within the CH_5 pool do not exchange, so that the CH_5 clusters with 5 protons in d_3-glycerol are preserved. The proton concentrations was kept below 10 M.

Figure 5A shows the T_M values extracted from experimental echo decays of these selectively isotope-labeled samples. (The echo decays are shown in the SI.) A clear dependence on pool type is observable. For the same total proton concentration, the system with CH_5 proton clusters has a shorter coherence time than the system with OH protons, and the system with a mixture of

both CH_5 proton clusters and OH protons falls in between. The simulations, also shown, correctly reproduce the observations. When the simulations are modified to only include proton pairs that are separated by more than 4 Å, decoherence slows down substantially and the differences between the three series vanish. This suggests that close proton pairs are responsible for decoherence and for the observed difference in decoherence between the different samples. This is consistent with You et al.'s studies on malonic acid crystals: their simulations identify geminal protons as the largest single contributor to central spin decoherence.[35]

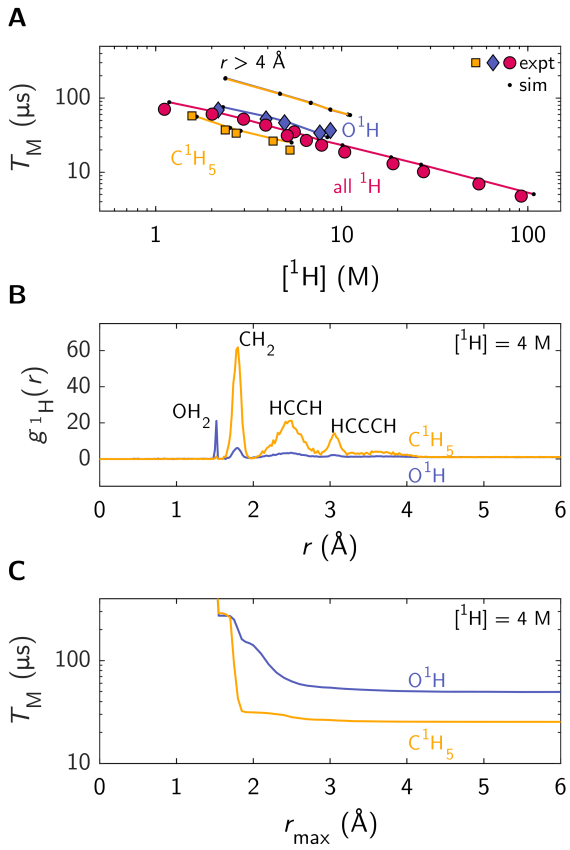

Figure 5: **A:** Coherence time versus proton concentration, both experimental (circles, diamonds, and squares) and simulated (dots), for all-H (red circles), CH_5 (yellow squares) and OH protiation (blue diamonds) are shown. The upper part of the plot shows simulations where only proton pairs with more than 4 Å separation are included. **B:** The ^{1}H–^{1}H radial distribution functions, $g(r)$, from the MD-simulated structure of solvated TEMPO, for the C^1H_5 and O^1H samples at $[^1\mathrm{H}] = 4$ M (96.5 % deuteration), plotted against ^{1}H–^{1}H distance r. The peaks are labeled by the proton pair type that is primarily responsible at that separation. **C:** Simulated decoherence time are shown versus maximum proton pair separation distance, r_{max}, for the same samples as in **B**. Since the coherence decays are not stretched exponentials for small r_{max} (see SI), T_{M} here is taken as the $1/\mathrm{e}$ decay time.

To investigate this further, Figure 5B shows the proton–proton rdfs for both O^1H and C^1H_5

samples with [^{1}H] = 4 M (96.5 % deuteration), as determined numerically from MD snapshots. (Note that the rdf for a sample with uniform 4 M deuteration differs from these two.) Both rdfs show multiple peaks at distances characteristic for various intra-molecular proton pairs (OH_2 at ≈1.5 Å, CH_2 at ≈1.8 Å, etc.). The peak for inter-molecular OH–OH overlaps with the HCCH peak. The rdf of the O^1H sample shows peaks at distances corresponding to CH_2 and HCCH. This is due to the 1 % protons in the CH pool. Except at the OH_2 distance, the rdf for the C^1H_5 sample is of larger magnitude than the one for the O^1H sample. The reason for this is that within a CH_5 proton cluster in d_3-glycerol, the relative probability of a second proton near a particular proton is high even at low bulk proton concentrations. In other words, the local CH proton concentration around a CH proton is more independent of the bulk concentration than that of the local OH concentration around a OH proton. Therefore, the C^1H_5 sample has a higher concentration of close proton pairs.

These close proton pairs are the main drivers of decoherence and the reason that decoherence is faster in the CH_5-protiated matrix than in the OH-protiated matrix. This is evident from Figure 5C, which shows T_Ms obtained from a series of simulations for both O^1H and C^1H_5 matrices again at [^{1}H] = 4 M (96.5 % deuterated). For T_M at a particular r_max, only proton pairs with a separation smaller than r_max were included. The calculated T_M of the C^1H_5 substitution sample shows a large drop at r_max corresponding to CH_2, demonstrating that these geminal proton pairs are the dominant decoherence drivers. In contrast, for the O^1H sample, protons pairs over a larger range of separations contribute to T_M, in part due to the fact that isotope scrambling reduces the number of geminal O^1H pairs. Therefore, in the O^1H sample, the contribution from the geminal OH_2 pairs is small, whereas the contributions from the CH_2 and HCCH pairs are comparable, but cumulatively smaller than in the CH_5 sample. This indicates that even in the O^1H sample, the 1 % non-exchangeable clustered protons are the dominant decoherence drivers.

The balance of magnetic dipolar couplings provides an explanation of how close proton pairs such as CH_2 drive decoherence. The analytical model of the Hahn echo modulation in an electron–proton–proton system[25] shows that the echo modulation depth from a proton pair (m, n) is maximal if the magnetic dipolar coupling strength among the protons $|b_{m,n}|$ matches the difference in electron–proton hyperfine couplings $|A_m - A_n|$, while the modulation frequency is proportional to their Pythagorean sum. The most significant proton pairs can be expected to be the ones with large enough $|b_{m,n}| \approx |A_m - A_n|$ for the modulations from similar clusters with slightly different modulation frequencies to become phase shifted with respect to each other within the timescale of the Hahn echo, and that occur in sufficient numbers. Clustering the protons in groups of five on the glycerols better achieves these conditions than uniformly scattering the protons throughout the sample.

In conclusion, the influence of matrix hydrogen isotope composition upon the electron spin decoherence dynamics of an organic radical in a frozen solid glassy matrix can be accurately predicted computationally and reveals several effects. Protons are the main decoherence drivers. Replacing protons with deuterons prolongs the coherence timescale. Large coherence time gains are only achieved at high levels of deuteration, $> 90\,\%$ ([^{1}H] < 10 M). Even in this regime, the coherence timescale is still primarily limited by the remaining protons rather than the numerically dominant deuterons. Furthermore, for a given concentration of protons, clustered protons are much stronger decoherence drivers than dispersed protons. Clustering leads to coherence times that do not follow an inverse-concentration dependence. Among proton clusters, those with separations < 2.5 Å are mainly responsible for the coherence loss. This means that both in EPR

experiments and in molecular and solid-state spin qubit architectures where long coherence times are required, special attention should be given to potential proton inclusions, in particular to geminal protons pairs, such as CH_2. In molecular systems, where protons are mostly unavoidable, declustering protons increases the coherence time, even while leaving the overall proton concentration the same. Similar conclusions should hold for other spin–1/2 nuclei (e.g. ^{13}C or ^{29}Si) in matrices where they dominate decoherence, although timescales will be different due to the different gyromagnetic ratios.

ASSOCIATED CONTENT

Supporting Information.

The Supporting Information is available free of charge on the ACS Publications website. It contains detailed descriptions of experimental parameters, molecular dynamics simulations, and spin quantum dynamics simulations.

AUTHOR INFORMATION

Corresponding Author

* ststst@uw.edu

Author Contributions

† S.M.J. and E.R.C. contributed equally to this work

ORCID

Samuel M. Jahn: 0000-0002-0197-681X
Elizabeth R. Canarie: 0000-0002-8393-3927
Stefan Stoll: 0000-0003-4255-9550

Notes

The authors declare no competing financial interests.

ACKNOWLEDGMENTS

This work was supported by the National Science Foundation (CHE-2154302, S.S.) and the National Institutes of Health (GM125753, S.S.). Parts of the spectrometer used in this work were funded by the National Institutes of Health (S10-OD021557, S.S.). E.R.C. was supported by the National Institute of General Medical Sciences of the NIH (T32-GM008268).

References

(1) Rowan, L. G.; Hahn, E. L.; Mims, W. B. Electron-Spin-Echo Envelope Modulation. *Phys. Rev.* **1965**, *137*, A61–A71.

(2) Mims, W. B. Envelope Modulation in Spin-Echo Experiments. *Phys. Rev. B* **1972**, *5*, 2409–2419.

(3) Larsen, R. G.; Singel, D. J. Double electron–electron resonance spin-echo modulation: Spectroscopic measurement of eletron spin pair separations in orientationally disordered solids. *J. Chem. Phys.* **1993**, *98*, 5134–5146.

(4) Milov, A. D.; Salikhov, K. M.; Tsvetkov, Y. D. Phase Relaxation of Hydrogen Atoms Stabilized in an Amorphous Matrix. *Sov. Phys. Solid State* **1973**, *15*, 802–806.

(5) Zecevic, A.; Eaton, G. R.; Eaton, S. S.; Lindgren, M. Dephasing of Electron Spin Echoes for Nitroxyl Radicals in Glassy Solvents by Non-Methyl and Methyl Protons. *Mol. Phys.* **1998**, *95*, 1255–1263.

(6) Committee on Technical Assessment of the Feasibility and Implications of Quantum Computing,; Computer Science and Telecommunications Board,; Intelligence Community Studies Board,; Division on Engineering and Physical Sciences,; National Academies of Sciences, Engineering, and Medicine, In *Quantum Computing: Progress and Prospects*; Grumbling, E., Horowitz, M., Eds.; National Academies Press: Washington, D.C., 2019; Pages: 25196.

(7) Gordon, J. P.; Bowers, K. D. Microwave Spin Echoes from Donor Electrons in Silicon. *Phys. Rev. Lett.* **1958**, *1*, 368–370.

(8) Graham, M. J.; Zadrozny, J. M.; Shiddiq, M.; Anderson, J. S.; Fataftah, M. S.; Hill, S.; Freedman, D. E. Influence of Electronic Spin and Spin–Orbit Coupling on Decoherence in Mononuclear Transition Metal Complexes. *J. Am. Chem. Soc.* **2014**, *136*, 7623–7626.

(9) Canarie, E. R.; Jahn, S. M.; Stoll, S. Quantitative Structure-Based Prediction of Electron Spin Decoherence in Organic Radicals. *J. Phys. Chem. Lett.* **2020**, *11*, 3396–3400.

(10) Soetbeer, J.; Hülsmann, M.; Godt, A.; Polyhach, Y.; Jeschke, G. Dynamical decoupling of nitroxides in o-terphenyl: a study of temperature, deuteration and concentration effects. *Phys. Chem. Chem. Phys.* **2018**, *20*, 1615–1628.

(11) Kveder, M.; Rakvin, B.; You, J. A Quantum Many Body Model for the Embedded Electron Spin Decoherence in Organic Solids. *J. Chem. Phys.* **2019**, *151*, 164124.

(12) Van Oort, E.; Glasbeek, M. Optically Detected Low Field Electron Spin Echo Envelope Modulations of Fluorescent N-V Centers in Diamond. *Chem. Phys.* **1990**, *143*, 131–140.

(13) Childress, L.; Gurudev Dutt, M. V.; Taylor, J. M.; Zibrov, A. S.; Jelezko, F.; Wrachtrup, J.; Hemmer, P. R.; Lukin, M. D. Coherent Dynamics of Coupled Electron and Nuclear Spin Qubits in Diamond. *Science* **2006**, *314*, 281–285.

(14) Balasubramanian, G.; Neumann, P.; Twitchen, D.; Markham, M.; Kolesov, R.; Mizuochi, N.; Isoya, J.; Achard, J.; Beck, J.; Tissler, J. et al. Ultralong spin coherence time in isotopically engineered diamond. *Nat. Mater.* **2009**, *8*, 383–387.

(15) Zadrozny, J. M.; Niklas, J.; Poluektov, O. G.; Freedman, D. E. Millisecond Coherence Time in a Tunable Molecular Electronic Spin Qubit. *ACS Cent. Sci.* **2015**, *1*, 488–492.

(16) Ward, R.; Bowman, A.; Sozudogru, E.; El-Mkami, H.; Owen-Hughes, T.; Norman, D. G. EPR distance measurements in deuterated proteins. *J. Magn. Reson.* **2010**, *207*, 164–167.

(17) Wedge, C. J.; Timco, G. A.; Spielberg, E. T.; George, R. E.; Tuna, F.; Rigby, S.; McInnes, E. J. L.; Winpenny, R. E. P.; Blundell, S. J.; Ardavan, A. Chemical Engineering of Molecular Qubits. *Phys. Rev. Lett.* **2012**, *108*, 107204.

(18) Lindgren, M.; Eaton, G. R.; Eaton, S. S.; Jonsson, B.-H.; Hammarström, P.; Svensson, M.; Carlsson, U. Electron spin echo decay as a probe of aminoxyl environment in spin-labeled mutants of human carbonic anhydrase II †. *J. Chem. Soc., Perkin Trans. 2* **1997**, 2549–2554.

(19) Huber, M.; Lindgren, M.; Hammarström, P.; Mårtensson, L.-G.; Carlsson, U.; Eaton, G.; Eaton, S. Phase memory relaxation times of spin labels in human carbonic anhydrase II: pulsed EPR to determine spin label location. *Biophys. Chem.* **2001**, *94*, 245–256.

(20) Klauder, J. R.; Anderson, P. W. Spectral Diffusion Decay in Spin Resonance Experiments. *Phys. Rev.* **1962**, *125*, 912–932.

(21) Zhidomirov, G. M.; Salikhov, K. M. Contribution to the Theory of Spectral Diffusion in Magnetically Diluted Solids. *Sov. Phys. J. Exp. Theor. Phys.* **1969**, *29*, 1037–1040.

(22) Hu, P.; Hartmann, S. R. Theory of Spectral Diffusion Decay Using an Uncorrelated-Sudden-Jump Model. *Phys. Rev. B* **1974**, *9*, 1–13.

(23) Brown, I. In *Time Domain Electron Spin Resonance*; Kevan, L., Schwartz, R., Eds.; John Wiley & Sons: New York, 1979; pp 195–229.

(24) Nevzorov, A. A.; Freed, J. H. A many-body analysis of the effects of the matrix protons and their diffusional motion on electron spin resonance line shapes and electron spin echoes. *J. Chem. Phys.* **2001**, *115*, 2416–2429.

(25) Witzel, W.; Das Sarma, S. Quantum theory for electron spin decoherence induced by nuclear spin dynamics in semiconductor quantum computer architectures: Spectral diffusion of localized electron spins in the nuclear solid-state environment. *Phys. Rev. B* **2006**, *74*, 035322.

(26) Saikin, S. K.; Yao, W.; Sham, L. J. Single-Electron Spin Decoherence by Nuclear Spin Bath: Linked-Cluster Expansion Approach. *Phys. Rev. B* **2007**, *75*, 125314.

(27) Kuprov, I.; Wagner-Rundell, N.; Hore, P. J. Polynomially Scaling Spin Dynamics Simulation Algorithm Based on Adaptive State-Space Restriction. *J. Magn. Reson.* **2007**, *189*, 241–250.

(28) Yang, W.; Liu, R.-B. Quantum many-body theory of qubit decoherence in a finite-size spin bath baths. *Phys. Rev. B* **2008**, *78*, 085315.

(29) Yang, W.; Liu, R.-B. Quantum many-body theory of qubit decoherence in a finite-size spin bath. II. Ensemble dynamics. *Phys. Rev. B* **2009**, *79*, 115320.

(30) Butler, M. C.; Dumez, J.-N.; Emsley, L. Dynamics of Large Nuclear-Spin Systems from Low-Order Correlations in Liouville Space. *Chem. Phys. Lett.* **209**, *477*, 377–381.

(31) Dumez, J.-N.; Butler, M. C.; Emsley, L. Numerical Simulation of Free Evolution in Solid-State Nuclear Magnetic Resonance Using Low-Order Correlations in Liouville Space. *J. Chem. Phys.* **2010**, *133*, 224501.

(32) Edwards, L. J.; Savostyanov, D. V.; Welderufael, Z. T.; Lee, D.; Kuprov, I. Quantum Mechanical NMR Simulation Algorithm for Protein-Size Spin Systems. *J. Magn. Reson.* **2014**, *243*, 107–113.

(33) Ma, W.-L.; Wolfowicz, G.; Zhao, N.; Li, S.-S.; Morton, J. J. L.; Liu, R.-B. Uncovering Many-Body Correlations in Nanoscale Nuclear Spin Baths by Central Spin Decoherence. *Nat. Commun.* **2014**, *5*, 4822.

(34) Lenz, S.; Bader, K.; Bamberger, H.; Van Slageren, J. Quantitative Prediction of Nuclear-Spin-Diffusion- Limited Coherence Times of Molecular Quantum Bits Based on Copper(II). *Chem. Commun.* **2017**, *53*, 4477–4480.

(35) You, J.; Carić, D.; Rakvin, B.; Štefanić, Z.; Užarević, K.; Kveder, M. Matrix Material Structure Dependence of the Embedded Electron Spin Decoherence. *J. Chem. Phys.* **2019**, *150*, 164124.

(36) Bahrenberg, T.; Jahn, S. M.; Feintuch, A.; Stoll, S.; Goldfarb, D. The Decay of the Refocused Hahn Echo in Double Electron–Electron Resonance (DEER) Experiments. *Magn. Reson.* **2021**, *2*, 161–173.

(37) Salikhov, K. M.; Dzuba, S. A.; Raitsimring, A. M. The Theory of Electron Spin-Echo Signal Decay Resulting from Dipole-Dipole Interactions between Paramagnetic Centers in Solids. *J. Magn. Reson.* **1981**, *42*, 255–276.

(38) Eaton, S. S.; Eaton, G. R. Relaxation Times of Organic Radicals and Transition Metal Ions. *Biol. Magn. Reson.* **2000**, *19*, 29–154.

(39) Abe, E.; Isoya, J.; Itoh, K. M. Pulsed EPR study of spin coherence time of P donors in isotopically controlled Si. *Physica B: Condens. Matter* **2006**, *376-377*, 28–31.

(40) Brown, I. M. Concentration Dependent Relaxation Times in Organic Radical Solids. *J. Chem. Phys.* **1973**, *58*, 4242–4250.

(41) Lunghi, A.; Sanvito, S. Electronic Spin-Spin Decoherence Contribution in Molecular Qubits by Quantum Unitary Spin Dynamics. *J. Magn. Magn. Mater.* **2019**, *487*, 165325.

(42) Maze, J. R.; Taylor, J. M.; Lukin, M. D. Electron Spin Decoherence of Single Nitrogen-Vacancy Defects in Diamond. *Phys. Rev. B* **2008**, *7*, 094303.

(43) Kanai, S.; Heremans, F. J.; Seo, H.; Wolfowicz, G.; Anderson, C. P.; Sullivan, S. E.; Galli, G.; Awschalom, D. D.; Ohno, H. Generalized Scaling of Spin Qubit Coherence in over 12,000 Host Materials. *arXiv* **2021**, *2102.02986*.

(44) Meiboom, S. Nuclear Magnetic Resonance Study of the Proton Transfer in Water. *J. Chem. Phys.* **1961**, *34*, 375–388.

(45) Agmon, N. The Grotthuss Mechanism. *Chem. Phys. Lett.* **1995**, *244*, 456–462.